minerals

MDPI

Article

The Solid Solution between $NaClO_3$ and $NaBrO_3$ Revisited

Florent Simon [1], Nicolas Couvrat [1], Christelle Bilot [2], Sylvain Marinel [2], Sylvie Malo [2] and Gérard Coquerel [1,*]

[1] SMS, UR 3233, University Rouen Normandie, 76000 Rouen, France; florent.rp.simon@gmail.com (F.S.); nicolas.couvrat@univ-rouen.fr (N.C.)
[2] ENSICAEN, UNICAEN, CNRS, CRISMAT, Normandie University, 14000 Caen, France; christelle.bilot@ensicaen.fr (C.B.); sylvain.marinel@ensicaen.fr (S.M.); sylvie.malo@ensicaen.fr (S.M.)
* Correspondence: gerard.coquerel@univ-rouen.fr

Abstract: $NaClO_3$ and $NaBrO_3$ are believed to form a complete solid solution from RT to fusion. The unique solid phase can thus be written: $NaClO_{3(1-x)}$-$NaBrO_{3(x)}$ with: $0 \leq x \leq 1$. This study shows that at high temperatures, this statement might be valid. Nevertheless, up to 50 °C, probably up to 160 °C, and even higher temperatures, this is not true when the system is in thermodynamic equilibrium. A large miscibility gap exists at room temperature (RT). This gap could be reduced up to a complete disappearance by fast crystallization, for instance, spray-drying. The necessary conditions to access equilibrium, including homochirality, are also discussed.

Keywords: solid solutions; heterogeneous stable & metastable equilibria; crystallization; sodium chlorate; sodium bromate

check for updates

Citation: Simon, F.; Couvrat, N.; Bilot, C.; Marinel, S.; Malo, S.; Coquerel, G. The Solid Solution between $NaClO_3$ and $NaBrO_3$ Revisited. *Minerals* **2023**, *13*, 1006. https://doi.org/10.3390/min13081006

Academic Editors: Nikita V. Chukanov and Vera N. Ermolaeva

Received: 20 June 2023
Revised: 13 July 2023
Accepted: 26 July 2023
Published: 28 July 2023

1. Introduction

1.1. General Concept of Solid Solutions and Motivations for the Choice of $NaClO_3$-$NaBrO_3$ System

Solid solutions by substitution are often encountered among inorganic and metallic systems as soon as the change between the two species can be simply the replacement of an atom by another atom with a close atomic radius. Often, in such a system, the lattice parameters of the solid solution for a given composition follow Vegard's rule, i.e., there is a linear relation between the lattice parameters of the crystal structure with the concentration of each of the components of the system [1]. However, this empirical law was not the general case, especially for metals [2,3].

Among inorganic solid solutions described in the literature, the $NaClO_3$-$NaBrO_3$ binary system (or $NaClO_3$-$NaBrO_3$-H_2O ternary system) has been widely investigated, especially as a relevant model for the study of deracemization [4–15], as well as an interesting case for the study crystal habit modification in the presence of impurities [16–23]. This may be partly due to the high crystallogenic character of the two components and their mixtures. Moreover, $NaClO_3$, $NaBrO_3$ and $NaClO_{3(x)}BrO_{3(1-x)}$ intermediate compositions have low melting points [24,25] and high (ClO_3-rich) to medium (BrO_3-rich) solubilities in water [20,26]. $NaClO_3$ has a melting point of 262 °C and a solubility in water of 790 $g.L^{-1}$. $NaBrO_3$ has a melting point of 347 °C and a solubility in water of 275 $g.L^{-1}$.

1.2. Crystal Structure of $NaClO_3$ and $NaBrO_3$ Pure Compounds and Chirality in the Solid State

Sodium chlorate ($NaClO_3$, MW = 106.44 $g.mol^{-1}$, T_{fus} = 262 °C) and sodium bromate ($NaBrO_3$, MW = 150.89 $g.mol^{-1}$, T_{fus} = 347 °C) have isomorphous crystal structures that were formerly investigated by Dickinson in 1921 [27]. Both halates crystallize in the chiral space group $P2_13$ (tetartohedral group in the cubic system), with crystallographic parameters a = 6.57584(5) and a = 6.70717(10) Angströms, respectively, at RT [28]. The space group $P2_13$ is chiral thus, noncentrosymmetric in adequation with the property to exhibit second-order nonlinear optical phenomena [29,30] (Savage, 1962; Simon, 1968).

$NaClO_3$ and $NaBrO_3$ belong to achiral ionic compounds that exhibit supramolecular chirality in the solid state [31]. It was also found that optically dextro (D) rotatory $NaClO_3$

has the opposite configuration than the optically dextro (D) rotatory $NaBrO_3$, or, in other words, $(NaClO_3)_D$ has the same structural configuration as $(NaBrO_3)_L$ [32–34]. Thus, the $(NaClO_3)_L/(NaClO_3)_D/(NaBrO_3)_L/(NaBrO_3)_D$ system is quaternary when the solid phases are considered.

1.3. $NaClO_{3(x)}BrO_{3(1-x)}$ Mixed Crystals: Kinetic Ordering and Deviation from Ideal Cubic Structure

In 1984, Raja et al. [35] analyzed a crystal with $Na(ClO_3)_{0.7}(BrO_3)_{0.3}$ composition and found that it crystallizes, also, in the cubic $P2_13$ space group, confirming the existence of the solid solution. Nevertheless, many other works indicated different results. Since the 19th century, polarized optical observations on $NaClO_{3(x)}BrO_{3(1-x)}$ solid solution crystals revealed birefringence that is physically not allowed in isotropic cubic structures [18,20,36]. The authors found that apparent single crystals exhibited sectors of different compositions (in both constituents of the solid solution), reducing the overall symmetry of these crystals to the monoclinic $P2_1$ or triclinic $P1$ space groups due to kinetic ordering of atoms during crystallization by water evaporation. Authors of the same research group also indicated the potential segregation of BrO_3^- and ClO_3^- microscale domains within an apparent 'single' crystal through alternating dextro- and levorotary domains [22]. A complete study of the $NaClO_{3(x)}BrO_{3(1-x)}$ system was also recently carried out by Su et al. [37]—crystals of the solid solution between 14 to 81 wt.% $NaBrO_3$ were found to be of worse optical quality, i.e., opaque with cracks contrary to crystals obtained outside this composition range. For these compositions, a very weak diffraction peak at 13.3° 2θ was found and could be indexed as the (100) peak, forbidden for the $P2_13$ space group (h00; h = 2n), indicating a slight deviation from an ideal cubic structure.

Nevertheless, it was reported that annealing close to the melting temperature leads to a homogenization of the crystals and a return to the $P2_13$ crystal structure [22,37,38]. It was not reported whether the $NaClO_{3(x)}BrO_{3(1-x)}$ solid solution crystals return to equilibrium or if a transition towards the cubic structure is only possible at higher temperatures and could remain metastable at room temperature.

1.4. Heterogeneous Equilibria

The first study of the $NaClO_3$-$NaBrO_3$ system was performed in 1939 by Swenson and Ricci [26], regardless of the chirality. They published two isothermal studies of the ternary system $NaClO_3$-$NaBrO_3$-H_2O at 25 °C and 50 °C (Figure 1a,c). They showed that there might be a complete solid solution between the two components at 50 °C (Figure 1d), but the possible existence of two solid solutions at 25 °C was envisaged (Figure 1b). Indeed, careful examinations of (i) the solubility curve versus composition and (ii) the tie lines in this isotherm at 25 °C reveal an odd behavior. In this work, the authors suggested that the solid solution was discontinuous. The solubility curve appeared to be divided into three parts corresponding to the following solid phases: (i) a solid solution very close to pure $NaBrO_3$, (ii) a bromate solid solution containing few ppm to 5–10% of chlorate, and (iii) a chlorate solid solution containing up to 60–65% chlorate solid solution. Another author suggested that this solid solution was continuous but with a marked tendency toward forming an isothermal invariant point.

1.5. Summary of the Literature Review and Aim of That Study

This literature review emphasizes the complex crystallization behavior by water evaporation for the $NaClO_3$-$NaBrO_3$ system, especially when the $NaClO_{3(x)}BrO_{3(1-x)}$ compositions are far from the respective pure phases. The problem is that crystallization is most often kinetically driven by the ability of ClO_3^-/BrO_3^- ions ordering and chirality ordering. Notably, both phenomena have been observed within an apparent well-shaped single crystal.

The question of whether the $NaClO_{3(x)}BrO_{3(1-x)}$ mixed crystals belong to a complete solution at room temperature (e.g., 25 °C) is finally still open. The reason might be that equilibrium seems to be challenging to reach.

Before examining the system regarding the chirality and deracemization of mixed compositions (in the next study), it appeared necessary to clarify the existence of heterogeneous equilibria between these two components.

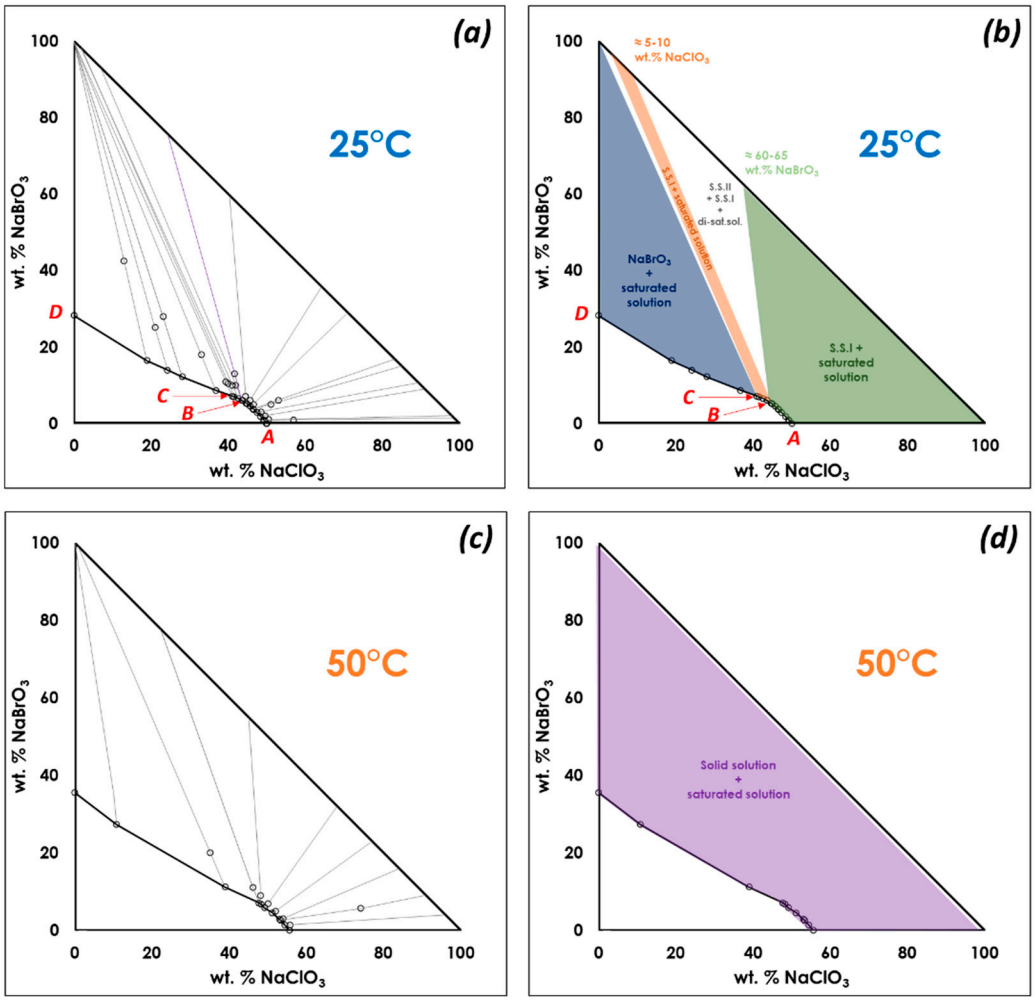

Figure 1. (**a**,**c**) Ternary isothermal sections at 25 °C and 50 °C proposed by Swenson and Ricci (adapted from ref. [26]) Note: No XRD data were collected during this work, the recovered solid compositions were determined by titration, so the interpretations of the data can be manifold. (**b**) Swenson and Ricci's proposal for biphasic domains (in accordance with the text and Table I in ref. [26]) in the ternary isotherm at 25 °C. At this temperature and in accordance with the Gibbs phase rule, those three biphasic domains need to be interlaced by triphasic domains (triangular white domains). The three regions are represented with different colors. The green domain encompasses, by far, the largest part of the two-phase region from 0% bromate (100% chlorate) to ca. 60–65 wt.% $NaBrO_3$ in the solid phase and from A to B for the corresponding saturated solution. The rather thin region, colored in grey, corresponds to a possible ordered domain ranging from 90–95% to almost 100% bromate in the solid phase and from B to C for the corresponding saturated solution. The last region colored in blue behaves like a pure component; the tie lines are likely to converge to nearly pure sodium bromate and the corresponding saturated solution ranging from C to D. (**d**) Swenson and Ricci's proposal for equilibria at 50 °C showing a continuous solid solution.

2. Material and Methods

2.1. Commercial Material

Sodium chlorate was purchased from Alfa Aesar with a purity of 99%. Sodium bromate was purchased from Merck with purity of 99%.

2.2. Crystallization by Solvent Evaporation

$NaClO_3$ and $NaBrO_3$ commercial powders were dissolved in water (40 mg/mL) to make undersaturated solutions of different $NaClO_3/NaBrO_3$ ratios. The solutions were transferred to individual opened large crystallization beakers for evaporation at RT or in a temperature-regulated ventilated oven. The crystals were collected at the end of evaporation to recover the same composition in $NaClO_3$ and $NaBrO_3$ that had been formerly introduced for the preparation of the samples. For some experiments at elevated temperatures, crystallizations were performed in opened vials under stirring.

2.3. Crystallization by Spray-Drying

The spray dryer used in this study is a Büchi B290 (conventional laboratory dryer designed with a co-current configuration). The compressed gas used is nitrogen, and the feeding solutions were aqueous. The laboratory-scale spray dryer was equipped with a nozzle 0.7 mm in diameter (Tip = 0.7 mm; Cap = 1.4 mm).

Several mixtures were dissolved in water, with the following parameters (Table 1).

Table 1. Spray-drying parameters for two sets of experiments.

Parameters	Protocol 1	Protocol 2
Concentration of the $NaClO_{3(1-x)}$-$NaBrO_{3(x)}$ aqueous solutions	2 g/150 mL water	6 g/50 mL water
The inlet temperature of the drying nitrogen	220 °C	220 °C
Feed flow rate (peristaltic pump)	360 mL/h	300 mL/h
The temperature of the feed solution	Room temperature	Ca. 60 °C
Atomizing airflow rate	473 L/h	500 L/h
Aspiration	40 m^3/h	40 m^3/h
Location of the powder at the end of the process	Mainly in the bowl collector	In the drying chamber, the cyclone and bowl collector

2.4. XRPD

XRPD patterns were obtained either with a Da Vinci D8 Bruker X-ray diffractometer with a Bragg-Brentano geometry (θ//θ) or a D8 diffractometer (Bruker, Germany) equipped with a modified goniometer of reverse-geometry (−θ/−θ) [39] (Coquerel, 2015). For both instruments, the incident X-ray beam consisted of the Cu Kα (λ = 1.5418 Å) with a tube voltage and amperage set at 40 kV and 40 mA, respectively. The diffraction patterns were collected with a LynxEye® linear detector (Bruker, Germany). Routine XRPD analyses were performed with a step of 0.04° (2θ) and a 12 s per step counting time from 3° to 30° (2θ). The system is monitored with DiffracPlus XRD commander software version 2.6.1. Data were processed with DIFFRAC.EVA software release 2018 (version 4.3.0.1).

2.5. TR-XRPD

Solid crystalline phases were analyzed by means of X-ray powder diffraction (XRPD) on a D8 advance series II diffractometer (Bruker Analytic X-ray Systems, Germany). The instrument has an X-ray tube containing a copper anticathode (40 kV, 40 mA) and a LynxEye® linear detector for every XRD scan. The step size was fixed at 0.04° with a counting time of 0.5 s/step over an angular range of 10°–40° (2-theta). The temperature was controlled and monitored using a TTK 450 heating stage (Anton Paar GmbH, Austria). Data were processed using DIFFRAC.EVA software release 2018 (version 4.3.0.1).

2.6. DSC

DSC experiments in the temperature range 0 °C to 400 °C were performed using a Netzsch DSC 204 F1 apparatus equipped with an intracooler. Each DSC run was performed

with ca. 5–15 mg of a powdered sample in aluminum pans with pierced lids at 2 or 5 K/min heating rates. The atmosphere of the analyses was regulated by a helium flux (40 mL/min). Onset (respectively endset) temperatures are calculated from the intersection between the baseline and the slope of the first (respectively last) part of the endotherm.

2.7. SEM

Scanning electron microscopy (SEM), pictures were obtained with a JEOL JCM-5000 NeoScope instrument (JEOL Ltd., Tokyo, Japan) (secondary scattering electron) at an accelerated voltage of 10 kV. Samples were stuck on an SEM stub with gloss carbon and coated with gold to reduce electric charges induced during analysis with a NeoCoater MP-19020NCTR (JEOL Ltd., Tokyo, Japan).

2.8. SEM-EDX

Scanning Electron Microscopy (JEOL JSM 7200F, JEOL Ltd., Tokyo, Japan) coupled with an Energy Dispersive X-ray spectrometer (EDX XFLASH 6160 from Bruker, Billerica, MA, USA) was used to collect images and for quantitative chemical analysis. EDS spectra were collected under a voltage of 10 kV with a working distance of 10 mm. Although no conductive coatings were deposited, the experimental conditions were satisfactory for recording BSE (Back Scattered Electrons) images and X-ray mapping experiments.

2.9. Optical Microscope

Polarized Optical Microscopy (POM) observation was conducted using a Nikon SMZ-10A microscope (Nikon Imaging Ltd., Tokyo, Japan) coupled to a CCD camera connected to a computer. Data processing was run by using LEICA Microsystems Application Suite X software (version 5.0.2.24429).

3. Results and Discussion

3.1. Confirmation of Kinetic Ordering through Classical (Slow) Water-Evaporation Crystallization Process Evidence of a Miscibility Gap at 20 °C

To confirm the existence of a complete solid solution, or by contrast, the presence of two limiting solid solutions with a miscibility gap, several 50 wt.% $NaClO_3$/$NaBrO_3$ mixtures in aqueous solutions were dissolved and left under stagnant conditions to fully evaporate at 20 °C, 50 °C, 80 °C, 100 °C, 120 °C and 150 °C. Two closely related XRPRD patterns were obtained (Figure 2). XRPD patterns of the 50 wt.% powder samples obtained after evaporation at room temperature indicated a miscibility gap in the solid state (Figure 2a), even though $NaClO_3$ and $NaBrO_3$ are isomorphous. A careful examination of the peaks of the powder samples crystallized at RT revealed that the two solid phases are not constituted by a physical mixture of pure $NaClO_3$ and pure $NaBrO_3$ but rather by a physical mixture of two solid solutions with a limiting domain of existence. How crystallization is conducted influences the apparent width in the composition of the solid solution. We suspect that rather robust metastable equilibria can be reached.

This miscibility gap was confirmed to exist (at least) up to 160 °C from the evaporation experiments conducted at elevated temperatures (Figure 2b).

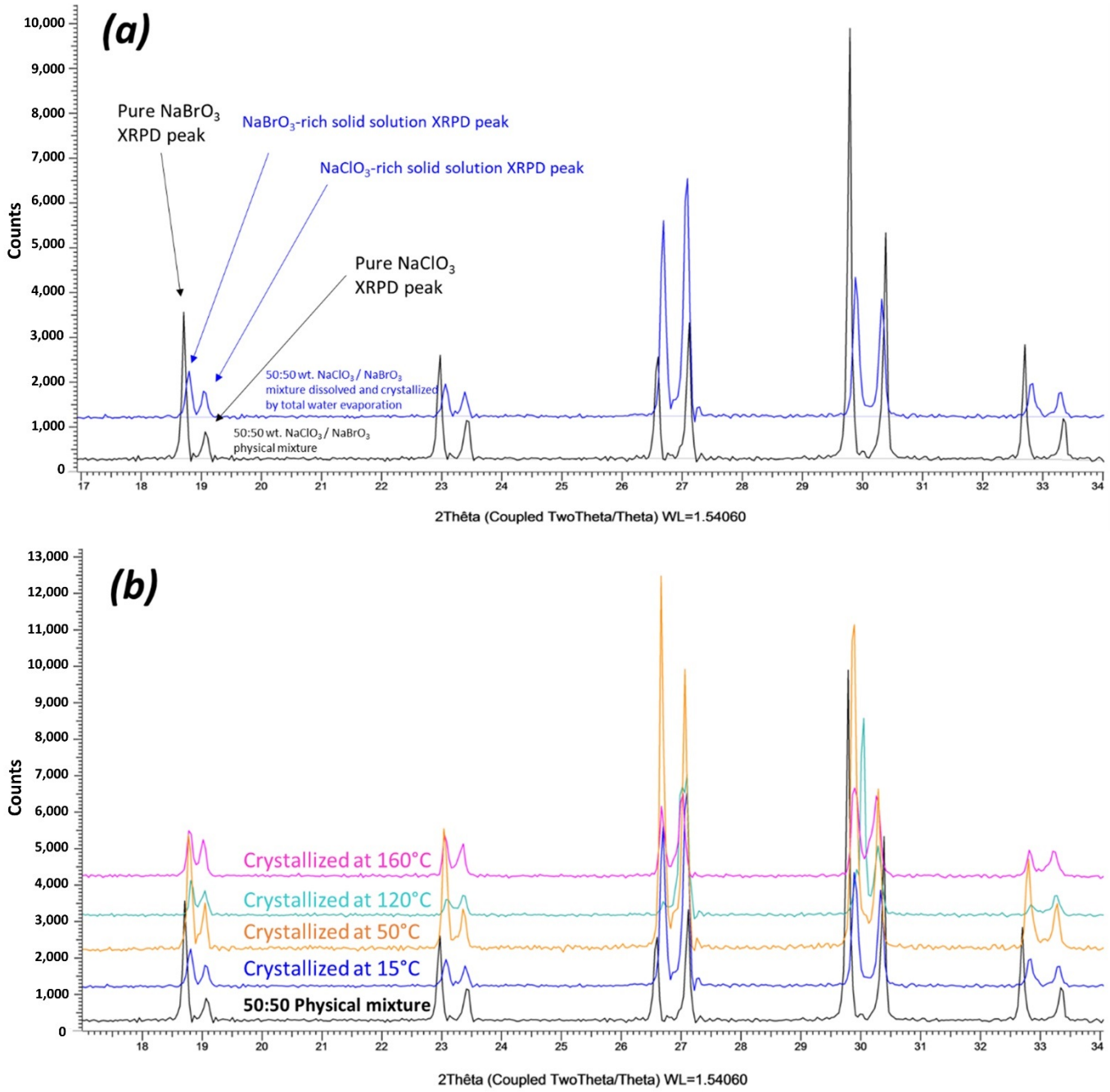

Figure 2. (**a**) XRPD pattern of powder sample (crystallized by slow evaporation under stirring from 50 wt.% $NaClO_3$/$NaBrO_3$ mixtures in aqueous solution) in comparison with pure $NaClO_3$ and $NaBrO_3$ (physical mixture). Two partial solid solutions exist: one $NaClO_3$-rich solid solution (S.S.I) and one $NaBrO_3$-rich solid solution (S.S.II). (**b**) XRPD patterns of powder samples crystallized by slow evaporation from 50 wt.% $NaClO_3$/$NaBrO_3$ mixtures in aqueous solution at different temperatures: RT, 15 °C, 50 °C, 120 °C, and 160 °C) confirmed that the miscibility gap is still present at elevated temperatures.

The crystallization pathway, from undersaturated solution towards total evaporation, was investigated on a 50 wt.% $NaClO_3$/$NaBrO_3$ mixture dissolved in water (Figure 3). During evaporation, several single particles were withdrawn at different times to investigate the solid phase. Results confirmed the solid-solid demixion (S.S.I + S.S.II + di-saturated saturated solution) during the last crystallization episodes.

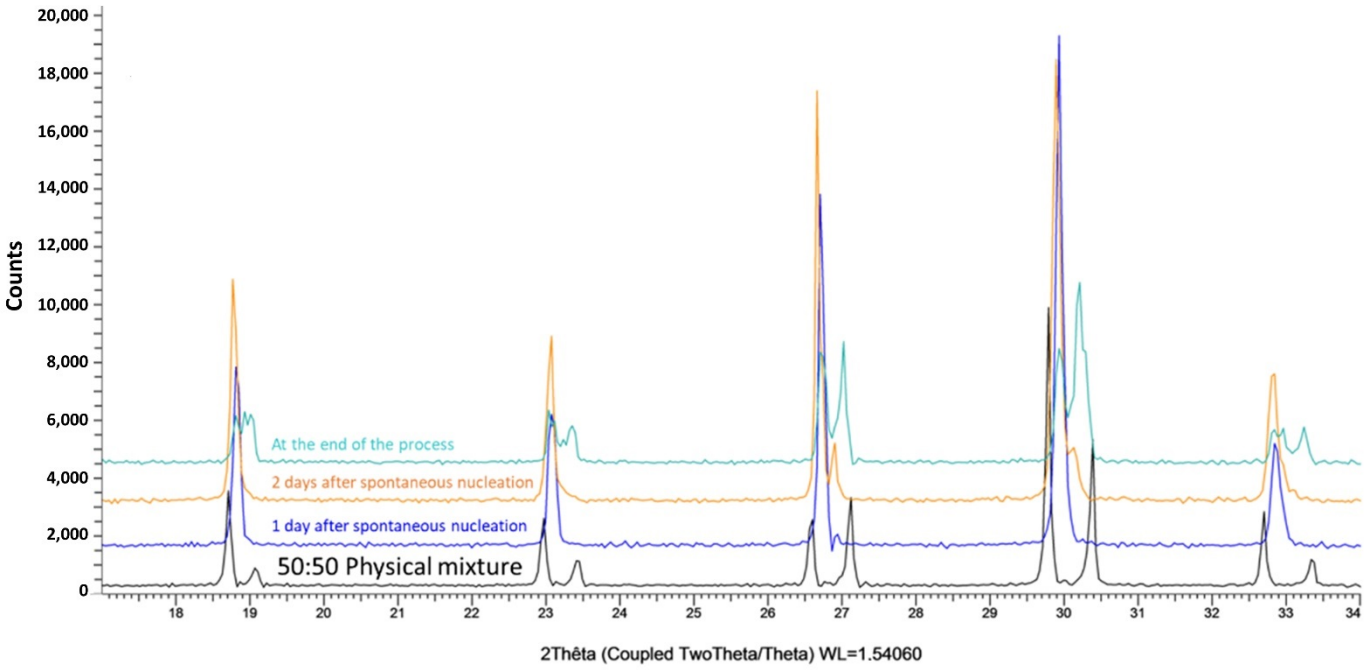

Figure 3. XRPD patterns of single particles withdrawn from an open crystallizer at different times during water evaporation: (black XRPD pattern): 50:50 $NaClO_3$/$NaBrO_3$ physical mixture (reference); (blue XRPD pattern) particle withdrawn after one day after spontaneous nucleation; (orange XRPD pattern) after two days after spontaneous nucleation; (green XRPD pattern) at the end of the process (total evaporation). Only one particle was withdrawn at a time, so the overall composition of the system remained unchanged.

Large crystals were obtained by water evaporation at 20 °C and submitted to a polarized microscopic inspection (Polarized Optical Microscopy: POM hereafter) (Figure 4) and SEM-EDX analysis (Figure 5).

POM pictures reveal that what appears as single particles are a patchwork of domains of different sizes and geometries. POM also shows that the chirality of those domains can differ even within the same crystallographic sector (Figure 4).

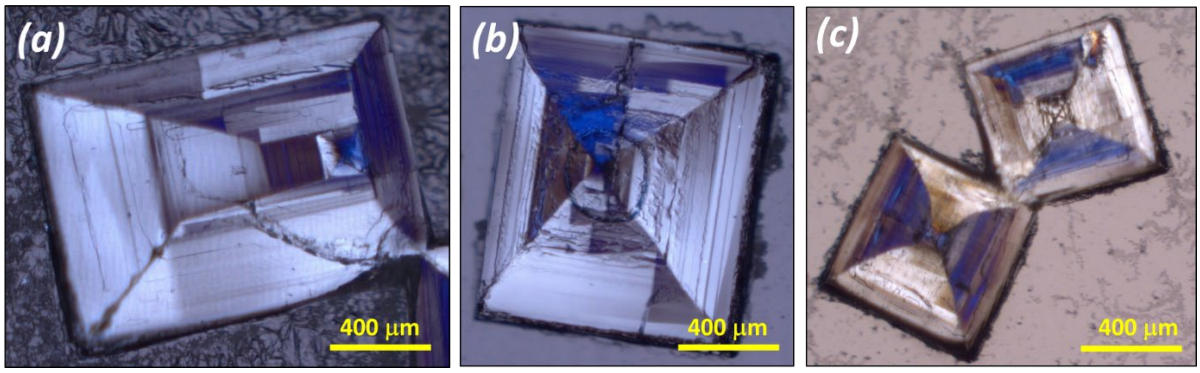

Figure 4. Polarized-light optical microscopy (POM) of selected $NaClO_{3(x)}BrO_{3(1-x)}$ mixed crystals grown by complete evaporation at 20 °C from 50 wt.% $NaClO_3$/$NaBrO_3$ mixtures in aqueous solution. (**a**–**c**) show single crystals revealing domains of different handedness. Hopper defects (concave crystals) were often found because crystal edges and corners grow faster than surfaces for large crystals grown at high supersaturation without stirring.

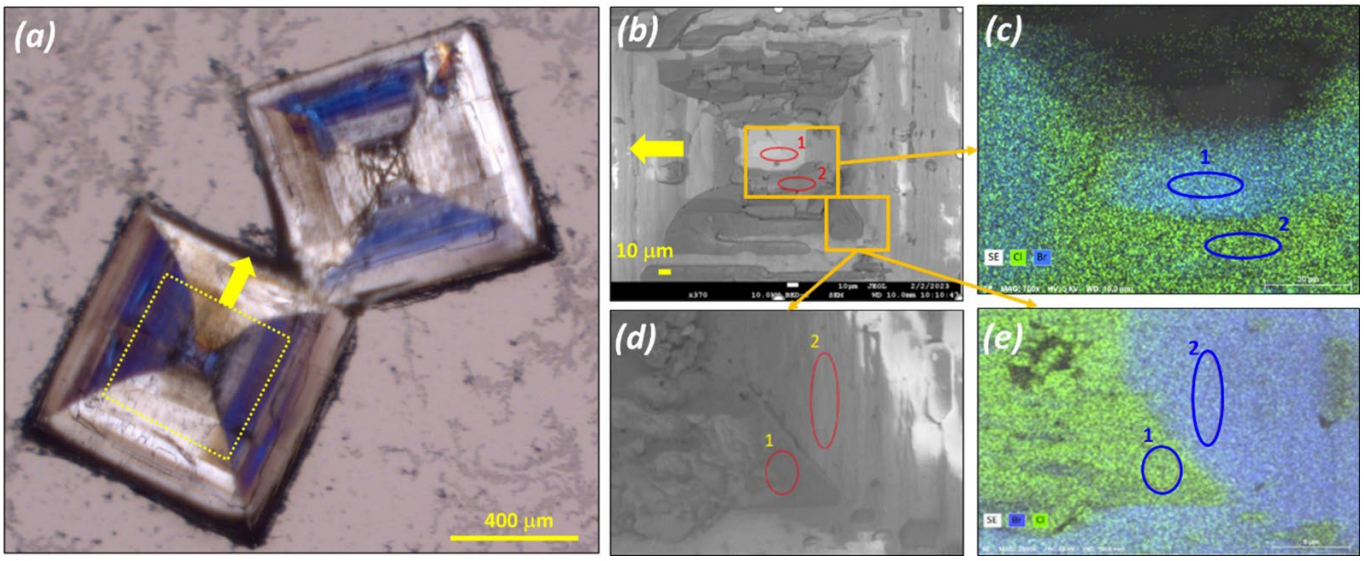

Figure 5. Mapping by EDX of a large particle obtained by slow aqueous evaporation at room temperature from a 50 wt.% $NaClO_3$/$NaBrO_3$. Mixture. (**a**) Polarized Optical Microscopy POM pictures showing the particle. (**b**,**d**) SEM pictures of a selected area of the selected particle. (**c**,**e**) corresponding composition mapping by EDX showing different concentrations of Cl and Br atoms depending on the selected zone on the particle: (**c**) zone 1: molar Br ratio = 30.5/(30.5 + 8.6) = 78%; zone 2: molar Br ratio = 20%; (**e**) zone 1: molar Br ratio = 21%; zone 2: molar Br ratio = 81%.

EDX analysis on two spots belonging to two domains reveals an almost inverted composition between Cl and Br (8.6 Cl & 30.5 Br atom % for spot 1) and (24.8 Cl and 6.2 Br atom % for spot 2). It can be surmised that those particles are composed of four domains: supramolecular left and right domains enriched in bromate and supramolecular left and right domains enriched in chlorate. Due to the poor solubility of the bromate compared to the chlorate, it is logical that the center of the particle is enriched in bromate. POM and EDX analyses were per many observations for this system in the literature [18,20,22,36,37].

From the above data, we can conclude that when the thermodynamic equilibrium is attained, sodium chlorate and sodium bromate do not form a complete solid solution from room temperature up to 160 °C, but rather two partial solid solutions. The miscibility gap in the solid state likely extends to much higher temperatures.

To see if the miscibility gap in the solid state intersects the solid-liquid equilibria, temperature, resolved X-ray powder diffraction experiments (TR-XRPD) were run for the 50% (mass) composition (Figure 6). Several heating ramps up to 250 °C were used on the same sample. With annealing for 11 h at high temperature, these thermal treatments were interspersed with a flattening of the powder to avoid the retreat effect of sintering.

Figure 6 shows the third analysis on heating. A careful inspection of the evolution of the diffraction peaks versus temperature indicates that the two patterns, related to the presence of a $NaClO_3$-rich and a $NaBrO_3$-rich solid solution, tend to coalesce into a single one. Even if the annealing temperature was close to that of the solidus (see experimental points (filled circles) in Figure 7), a genuine complete merge of the two patterns is not observed. Longer annealing has shown the beginning of decomposition and, therefore, could not be prolonged. The opposite supramolecular chirality of the particle may not help the sintering. Thus, this work leads to two hypotheses shown in Figure 7a,b.

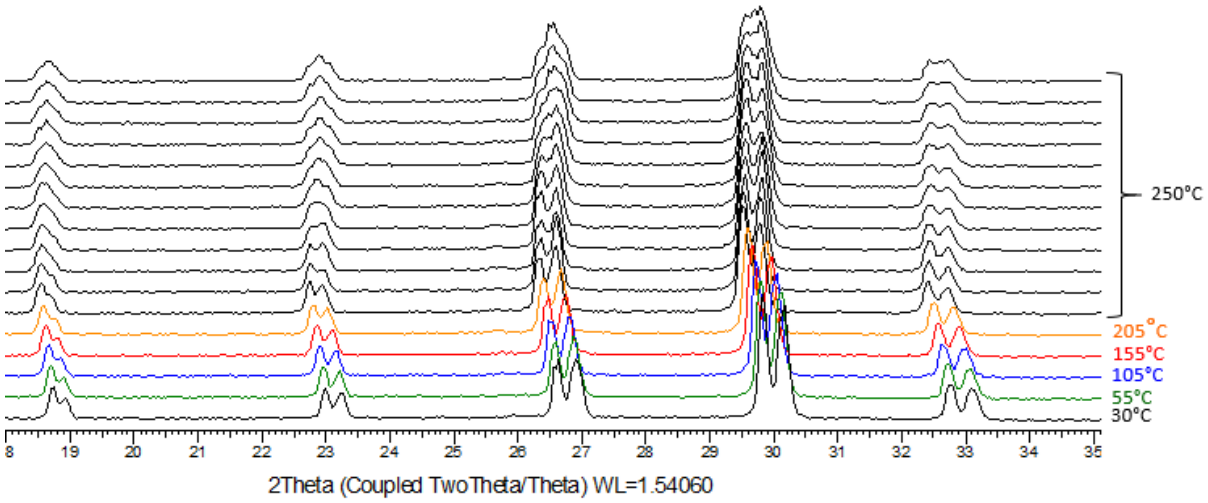

Figure 6. TR-XRPD of a 50% Mass Composition from 85 °C to 250 °C, annealing the 11 last patterns (11 h) at 250 °C.

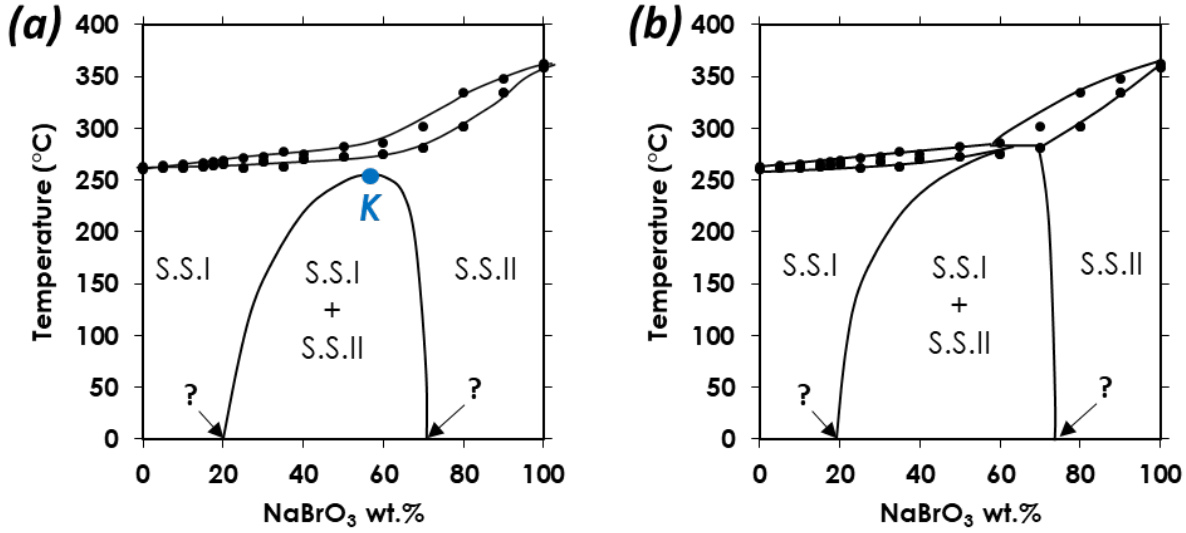

Figure 7. (**a**) Tentative homochiral binary phase diagram between $NaClO_3$ and $NaBrO_3$ showing a stable miscibility gap up to a critical point (K), above which a long period of diffusion time could succeed in mixing the two components in the full range of composition (i.e., from 0 to 100% $NaBrO_3$). Note that homochirality is supposed to appear to give left-handed or right-handed crystals only. (**b**) Tentative homochiral binary phase diagram between $NaClO_3$ and $NaBrO_3$ showing a stable miscibility gap that does not close up at elevated temperature but intersects the liquid-solid equilibria, implying a three-phase invariant (peritectic transition). Note: for both (**a**,**b**), filled circles correspond to experimental points determined by DSC (present work). Question marks, on *x* axis, reflect the difficulties to find the precise limits of the miscibility gap for stable equilibria.

3.2. Crystallization of $NaClO_3$/$NaBrO_3$ Mixtures by Spray-Drying. Evidence of a Metastable Complete Solid Solution

Literature shows that homogeneity could be an issue in preparing samples with different compositions. Therefore, mixtures $NaClO_{3(x)}BrO_{3(1-x)}$ $0 \leq x \leq 1$ have been prepared by spray-drying according to Protocol 1.

It can be surmised that in every droplet, a Kondepudi-like crystallization occurs. Accordingly, every droplet should give homochiral particles on drying unless there is a bias in the nucleation process due to an active chiral impurity. The global result should be the statistical nucleation of right-handed and left-handed particles, in other words: a racemic mixture. A recent article discussed the relationship between size and homochirality [40].

The obtained particles exhibit morphologies more isotropic than crystallization from stagnant solution for which the habitus is flattened with characteristic defects (Figure 8).

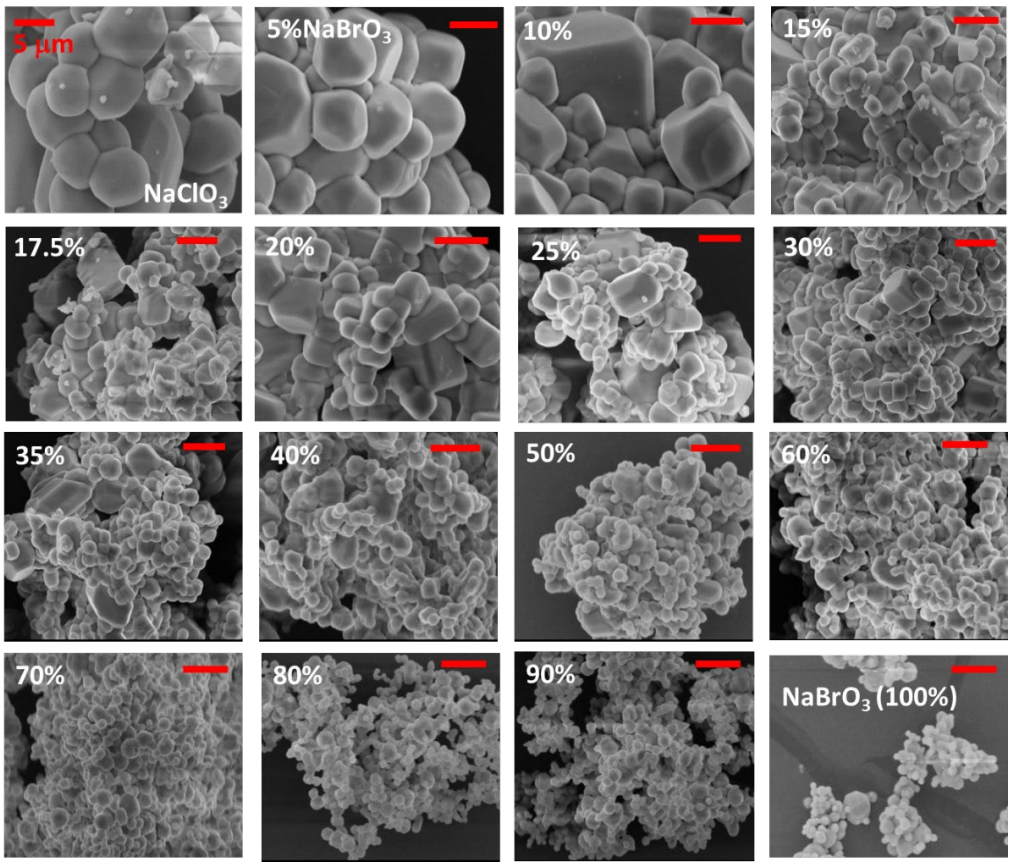

Figure 8. SEM pictures—with the same magnification- of spray-dried samples obtained by using Protocol 1 from different initial compositions (ranging from 0% $NaBrO_3$ (100% $NaClO_3$) to 100% $NaBrO_3$ (0% $NaClO_3$)). As $NaBrO_3$ is less soluble than $NaClO_3$, the particles were smaller.

XRPD patterns on fresh spray-dried samples recorded at room temperature are shown in Figure 9. Contrary to powder samples obtained by slow water evaporation, the inlet shows the shift of the X-ray diffraction peak versus composition in the full composition range $0 \leq x \leq 1$.

The evolution of the cubic unit-cell parameter at room temperature as a function of the mole fraction of $NaBrO_3$ is represented in Figure 10. Although the maximum difference between $NaClO_3$ and $NaBrO_3$ lattice parameters is only 1.92%, a possible slight deviation from the Vegard law seems to be observable, which could be related to the metastable character of the complete solid solution. More accurate measurements would be necessary to confirm the non-Vegard trend close to the pure components in the domain of stable partial solid solutions.

The solid mixtures obtained by spray-drying (Protocol 1) were analyzed by DSC at a 5 K/min heating rate. Figure 11a shows the profiles versus composition on heating, and Figure 11b collects the onset and endset of the melting peak (solid-filled circles). The resulting binary system includes a solidus and a liquidus which are rather flat up to 60 wt.% $NaBrO_3$. This seems consistent with the tie-lines of the ternary system at 25 °C determined by Swenson and Ricci [26]. The binary system is consistent with a continuous solid solution by means of substitution.

To increase spray-drying productivity, a mixture of 50% (mass) was used with protocol 2 (concentration eight times higher than protocol 1 and the temperature of the feeding liquid was 60 °C). With these new parameters, part of the solid was stuck on the upper part of the drying chamber. The rest was stuck on the outlet of the drying chamber or in the collector bowl.

XRPD analyses of the solid in the drying chamber and the collector bowl are displayed in Figure 12 (The solid stuck at the outlet of the drying chamber appeared identical to that in the collector bowl). The two XRPD patterns show a clear difference: (i) the powder stuck in the upper part of the drying chamber is duplicated, testifying the presence of two similar solid solutions (ii) the powder sampled from the collector bowl is a single phase with diffraction peaks having intermediate d-spacings in comparison with the two partial solid solutions. For the former, the full and fast dehydration of the droplets is aborted, resulting in two solid solutions. For the latter, a fast and completed dehydration leads to a unique solid solution with the same composition as the feeding solution. This solid is the same result as when using protocol 1.

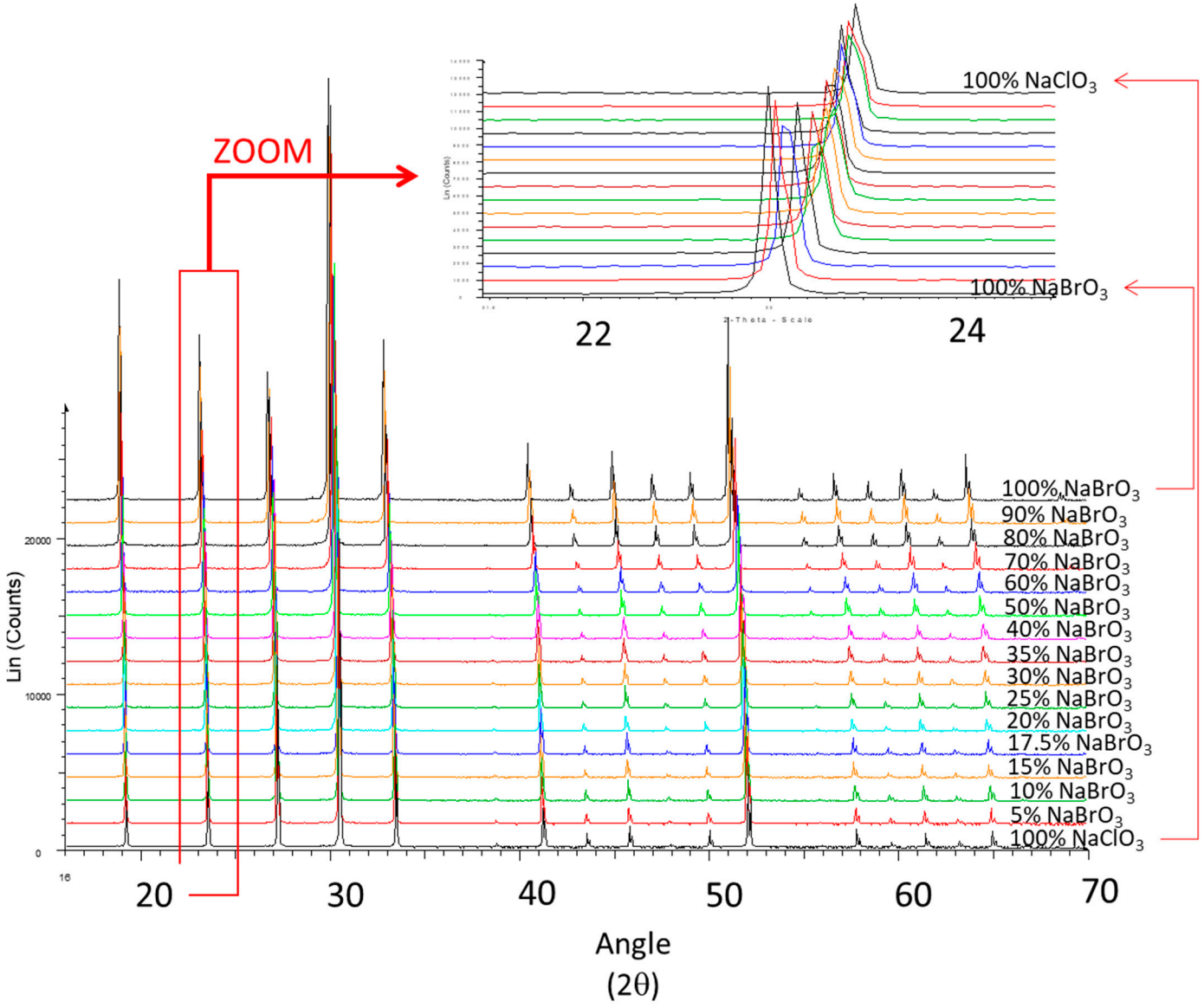

Figure 9. XRPD pattern versus composition of $NaClO_{3(x)}BrO_{3(1-x)}$ (mass fraction) prepared by spray-drying-protocol 1-The inlet is a zoom on the second peak at ca. 23 ° (2θ scale Cu Kα).

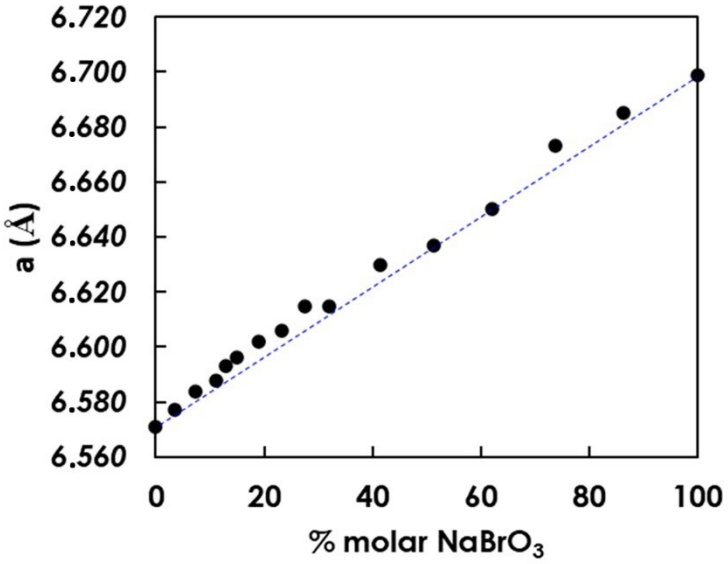

Figure 10. Crystallographic parameter **a** of the complete metastable solid solution $NaClO_{3(x)}BrO_{3(1-x)}$ (molar fraction) prepared by spray-drying -using protocol 1 (precise values are reported in Table S1). A deviation from the Vegard law (apparent non-linearity) seems present for some compositions. The blue line is for guiding the eyes.

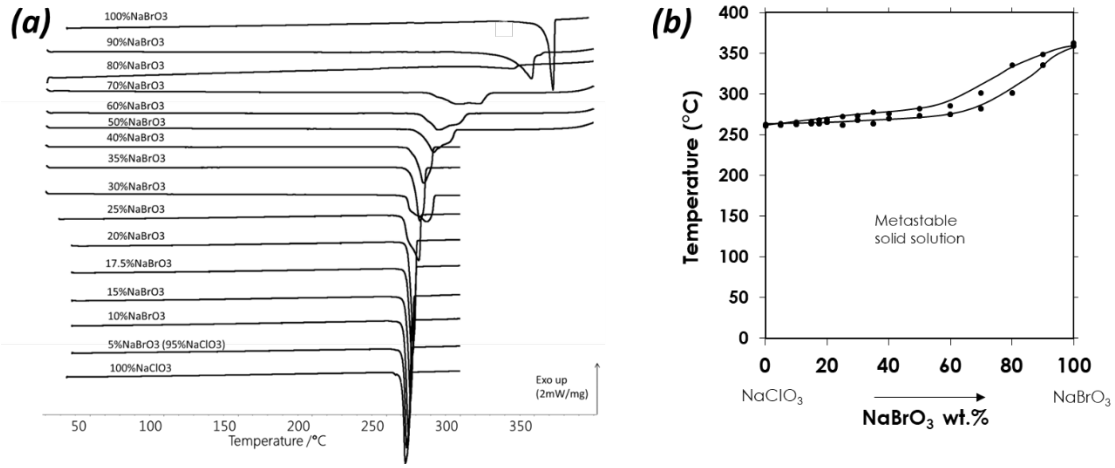

Figure 11. (**a**) DSC analyses (heating rate 5 $K.min^{-1}$) of powder samples prepared by spray-drying (Protocol 1). (**b**) Racemic binary section of the quaternary system: $(NaClO_3)_L/(NaClO_3)_D/(NaBrO_3)_L/(NaBrO_3)_D$. for which a metastable solid solution could be obtained.

If the powder obtained after spray-drying in the collector bowl is put for one day under 84% relative humidity at RT, the single XRPD signature spits into two resembling XRPD patterns, just like what is obtained by complete slow evaporation.

These results demonstrate that, whatever the composition, the two components could be forced to mix completely if the kinetics of crystallization is fast enough and if the drying is completed in a single step, such as during spray-drying using protocol 1. Of course, under these conditions, homochirality cannot be controlled; the final product is a random distribution of chiral particles -probably close to a racemic mixture. Thus, the binary section presented in Figure 11b is merely a metastable racemic section of the quaternary system: $NaClO_3$\\-$NaClO_3$//- $NaBrO_3$\\-$NaBrO_3$//, The symbols: \\ and//refer to opposite supramolecular chirality. The crystallographic features of the two components: the same space group, and a small difference only of the cubic parameter (less than 2% at RT), render possible the existence of two mirror-image metastable complete solid solutions.

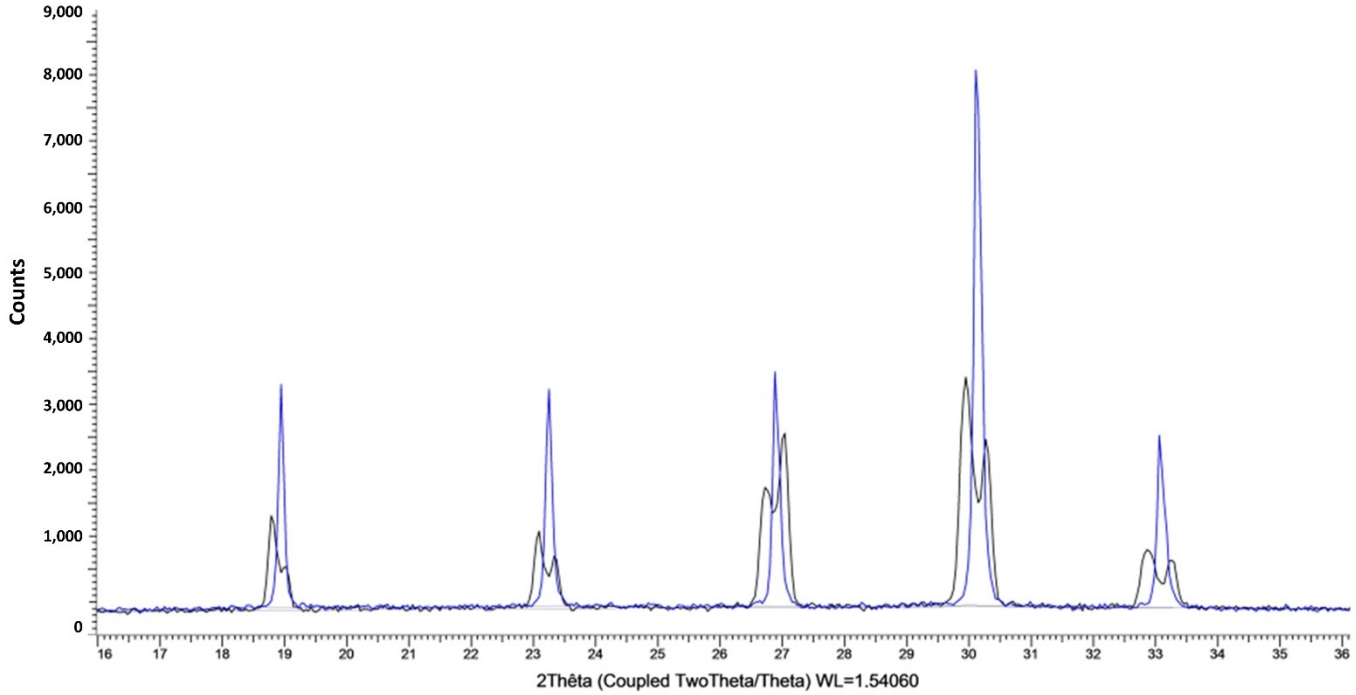

Figure 12. 50% mass after Spray drying protocol 2: (black pattern) solid collected in the upper part of the drying chamber; (blue pattern): solid from the collector bowl.

4. Conclusions & Perspectives

Spray-drying is a technique which favorizes access to metastable states because the entire crystallization—including nucleation, growth, and complete drying—takes place in the order of one second. Using this energetic and swift process, the sodium chlorate and sodium bromate appear fully miscible from RT to fusion. However, the two-mirror-image complete solid solutions are actually in a metastable state. Strangely enough, the metastable part of the solid solution corresponds to a slightly denser crystal lattice than the mean of the two stable limiting solid solutions. When the relative humidity exceeds a threshold of ca. 75–84%, the two (lefthanded and righthanded) complete solid solutions spit into mirror-image partial solid solutions.

For larger particles, such as those obtained by slow evaporation without stirring, this work evidences the presence of domains rich in bromate and others rich in chlorate, which have epitaxial relationships. For solid solutions grown from stirred solutions, the composition ranges of the two limited solid solutions are difficult to assess. On the one hand, spray-drying experiments and, on the other hand, EDX analyses of composition in different sectors of single particles are consistent with these fluctuations.

The construction of the genuine stable phase diagram does not appear that straightforward. Indeed, in addition to the formations of the partial solid solutions, it is necessary to reach homochirality. This could be ensured by continuous grinding (but the pollution by material snatched off from the beads could be an issue) or temperature cycling assisted or not by ultrasounds. The kinetics of attaining the 'true' equilibrium depends on the doses of those treatments (i.e., intensity versus time).

Future work will focus on the deracemization of $NaClO_3$-rich solid solution and $NaBrO_3$-rich solid solution up to their limits in compositions. It will also be interesting to test the deracemization inside the miscibility gap of these two partial solid solutions. Is there an influence of the two ss$NaClO_3$ rich and ss$NaBrO_3$ rich to reach identical supramolecular chirality so: homo-homochirality or, by contrast: hetero-homochirality?

Supplementary Materials: The following supporting information can be downloaded at: https://www.mdpi.com/article/10.3390/min13081006/s1, Figure S1: XRPD of ground $NaClO_3$/$NaBrO_3$ physical mixture (black) and XRPD of unground $NaClO_3$/$NaBrO_3$ physical mixture (blue); Table S1: Refined average parameter versus composition of the solid solution obtained by Spray-Drying with protocol 1. Measurements at RT.

Author Contributions: Conceptualization, G.C.; Data curation, S.M. (Sylvain Marinel); Investigation, F.S., N.C., C.B. and G.C.; Methodology, G.C.; Resources, S.M. (Sylvie Malo); Writing—original draft, F.S. and G.C.; Writing—review & editing, G.C. All authors have read and agreed to the published version of the manuscript.

Funding: This research received no external funding.

Data Availability Statement: On request, raw data are available from the corresponding author.

Conflicts of Interest: The authors declare no conflict of interest and agree on the last version of the manuscript.

References

1. Vegard, L. The constitution of the solid solution and the space filling of the atoms. *Z. Phys.* **1921**, *5*, 17–26. [CrossRef]
2. King, H.W. Qualitative size-factors for metallic solid solutions. *J. Mater. Sci.* **1966**, *1*, 79–90. [CrossRef]
3. Denton, A.R.; Ashcroft, N.W. Vegard's law. *Phys. Rev. A* **1991**, *43*, 3161–3164. [CrossRef]
4. Kipping, F.S.; Pope, W.J. Enantiomorphism. *J. Chem. Soc. Trans.* **1898**, *73*, 606–617. [CrossRef]
5. Kondepudi, D.K.; Kaufman, R.J.; Singh, N. Chiral symmetry breaking in sodium chlorate crystallization. *Science* **1990**, *250*, 975–976. [CrossRef] [PubMed]
6. Kondepudi, D.K.; Prigogine, I. Sensitivity of nonequilibrium systems. *Phys. A Stat. Mech. Appl.* **1981**, *107*, 1–24. [CrossRef]
7. Kondepudi, D.K.; Nelson, G.W. Chiral symmetry breaking in nonequilibrium systems. *Phys. Rev. Lett.* **1983**, *50*, 1023–1026. [CrossRef]
8. Kondepudi, D.K.; Nelson, G.W. Weak neutral currents and the origin of biomolecular chirality. *Nature* **1985**, *314*, 438–441. [CrossRef]
9. Buhse, T.; Durand, D.; Kondepudi, D.; Laudadio, J.; Spilker, S. Chiral symmetry breaking in crystallization: The role of convection. *Phys. Rev. Lett.* **2000**, *84*, 4405–4408. [CrossRef]
10. Viedma, C. Chiral symmetry breaking during crystallization: Complete chiral purity induced by nonlinear autocatalysis and recycling. *Phys. Rev. Lett.* **2005**, *94*, 065504. [CrossRef]
11. Suwannasang, K.; Flood, A.; Rougeot, C.; Coquerel, G. Using Programmed Heating-Cooling with Racemization in Solution for Complete Symmetry Breaking of a Conglomerate Forming System. *Cryst. Growth Des.* **2013**, *13*, 3498–3504. [CrossRef]
12. Rougeot, C.; Guillen, F.; Plaquevent, J.-C.; Coquerel, G. Ultrasound-Enhanced Deracemization: Towards the Existence of Agonist Effects in the Interpretation of Spontaneous Symmetry Breaking. *Cryst. Growth Des.* **2015**, *15*, 2151–2155. [CrossRef]
13. Viedma, C.; Cintas, P. Homochiraliry beyond grinding: Deracemizing chrial crystals by temperature gradient under boiling. *Chem. Commun.* **2011**, *47*, 12786–12788. [CrossRef] [PubMed]
14. Viedma, C.; McBride, J.M.; Kahr, B.; Cintas, P. Enantiomeric-Specific Oriented Attachment: Formation of Macroscopic Homochiral Crystal Aggregates from a Racemic System. *Angew. Chem. Int. Ed.* **2013**, *52*, 10545–10548. [CrossRef] [PubMed]
15. Schindler, M.; Brandel, C.; Kim, W.-S.; Coquerel, G. Temperature Cycling Induced Deracemization of $NaClO_3$ under the Influence of $Na_2S_2O_6$. *Cryst. Growth Des.* **2020**, *20*, 414–421. [CrossRef]
16. Buckley, H.E. 2. The Influence of RO_4 and Related Ions on the Crystalline Form of Sodium Chlorate. *Z. Krist.* **1930**, *75*, 15–31.
17. Ristic, R.; Sherwood, J.N.; Wojciechowskf, K. Morphology and growth kinetics of large sodium chlorate crystals grown in the presence and absence of dithionate impurity. *J. Phys. Chem.* **1993**, *97*, 10774–10782. [CrossRef]
18. Gopalan, P.; Peterson, M.L.; Crundwell, G.; Kahr, B. Reevaluating Structures for Mixed Crystals of Simple Isomorphous Salts: $NaCl_xBr_{1-x}O_3$. *J. Am. Chem. Soc.* **1993**, *115*, 3366–3367. [CrossRef]
19. Ristic, R.; Shekunov, B.Y.; Sherwood, J.N. Growth of the tetrahedral faces of sodium chlorate crystals in the presence of dithionate impurity. *J. Cryst. Growth* **1994**, *139*, 336–343. [CrossRef]
20. Crundwell, G.Y.; Gopalan, P.; Bakulin, A.; Peterson, M.L.; Kahr, B. Effect of Habit Modification on Optical and X-ray Structures of Sodium Halate Mixed Crystals: The Etiology of Anomalous Double Refraction. *Acta Cryst.* **1997**, *B53*, 189–202. [CrossRef]
21. Kahr, B.; Gurney, R.W. Dyeing crystals. *Chem. Rev.* **2001**, *101*, 893–951. [CrossRef] [PubMed]
22. Kaminsky, W.; Claborn, K.; Kahr, B. Polarimetric imaging of crystals. *Chem. Soc. Rev.* **2004**, *33*, 514–525. [CrossRef]
23. Lan, Z.-P.; Lai, X.; Roberts, K.; Klapper, H. X-ray Topographic and Polarized Optical Microscopy Studies of Inversion Twinning in Sodium Chlorate Crystals Grown in the Presence of Sodium Dithionate Impurities. *Cryst. Growth Des.* **2014**, *14*, 6084–6092. [CrossRef]
24. Chandrasekaran, K.S.; Monhanlal, S.K. The X-ray anomalous dispersion and optical rotation in the crystalline solid solution $NaClO_3$: $NaBrO_3$. *Pramana* **1976**, *7*, 152–159. [CrossRef]

25. Subhadra, K.G.; Hussain, K.A. Melting Temperatures of $NaClO_3$-$NaBrO_3$ Mixed Crystals. *Cryst. Res. Technol.* **1987**, *22*, 827–833. [CrossRef]
26. Swenson, T.; Ricci, J.E. The Ternary Systems $KBrO_3$-$KClO_3$-H_2O at 25 °C and $NaBrO_3$-$NaClO_3$-H_2O at 25 and 50 °C. *J. Am. Chem. Soc.* **1939**, *61*, 1974–1977. [CrossRef]
27. Dickinson, R.G.; Goodhue, E.A. The Crystal Structure of Sodium Chlorate and Sodium Bromate. *J. Am. Chem. Soc.* **1921**, *43*, 2045–2055. [CrossRef]
28. Abrahams, S.C.; Bernstein, J.L. Remeasurement of Optically Active $NaClO_3$ and $NaBrO_3$. *Acta Cryst.* **1977**, *B33*, 3601–3604. [CrossRef]
29. Savage, A.; Miller, R.C. Measurements of Second Harmonic Generation of Ruby Laser Line in Piezoelectric Crystals. *Appl. Opt.* **1962**, *1*, 661–664. [CrossRef]
30. Simon, H.J.; Bloembergen, N. Second-Harmonic Light Generation in Crystals with Natural Optical Activity. *Phys. Rev.* **1968**, *171*, 1104–1114. [CrossRef]
31. Matsuura, T.; Koshima, H. Review: Introduction to chiral crystallization of achiral compounds. Spontaneous generation of chirality. *J. Photochem. Photobiol.* **2005**, *6*, 7–24. [CrossRef]
32. Ramachandran, G.N.; Chandrasekaran, K.S. The Absolute Configuration of Sodium Chlorate. *Acta Crystallogr.* **1957**, *10*, 671–675. [CrossRef]
33. Beurskens-Kerssen, G.; Kroon, J.; Endeman, H.J.; Van Laar, J.; Bijvoet, J.M. Absolute Configuration and Rotatory Power of the Crystals of $NaBrO_3$ and $NaClO_3$. In *Crystallography and Crystal Perfection*; Academic Press Inc.: Cambridge, MA, USA, 1963; pp. 225–236.
34. Chandrasekhar, S.; Madhava, M.S. Optical roratory dispersion of crystals of sodium chlorate and sodium bromate. *Acta Cryst.* **1967**, *23*, 911. [CrossRef]
35. Sanjeevi Raja, C.; Mohanlal, S.K.; Chandrasekaran, K.S. An X-ray diffraction study of the size effect on a crystalline solid solution of sodium halates. *Z. Krist.* **1984**, *166*, 121–127.
36. Shtukenberg, A.G.; Rozhdestvenskaya, I.V.; Popov, D.Y.; Punin, Y.O. Kinetic ordering of atoms in sodium chlorate-bromate solid solutions. *J. Solid State Chem.* **2004**, *177*, 4732–4742. [CrossRef]
37. Su, J.; Song, Y.; Zhang, D.; Chang, X. Characterization of unidirectionally grown $NaCl_{1-x}Br_xO_3$ crystals. *Powder Diffr.* **2009**, *24*, 234–238. [CrossRef]
38. Hulliger, J.; Wüst, T.; Brahimi, K.; Burgener, M.; Aboufadl, H. A stochastic principle behind polar properties of condensed molecular matter. *New J. Chem.* **2013**, *37*, 2229–2235. [CrossRef]
39. Coquerel, G.; Sanselme, M.; Lafontaine, A. Method and Measuring Scattering of X-rays, Its Applications and Implementation. Device. Patent EP2694953A1, 12 February 2012.
40. Bak, S.Y.; Coquerel, G.; Kim, W.-S.; Park, B.J. Solution Volume Effects on Spontaneous Chiral Symmetry Breaking of Sodium Chlorate Crystals. *J. Phys. Chem. Lett.* **2023**, *14*, 785–790. [CrossRef]